

An Orbifold Framework for Classifying Layer Groups with an Application to Knitted Fabrics

Sonia Mahmoudi,^{1, 2, 3,*} Elizabeth J. Dresselhaus,⁴ and Michael S. Dimitriev⁵

¹Advanced Institute for Materials Research (WPI-AIMR), Tohoku University,
2-1 Katahira, Aoba-ku, Sendai, Miyagi 980-8577, Japan

²RIKEN, Center for Interdisciplinary Theoretical and Mathematical Sciences (iTHEMS), 2-1, Hirosawa, Wako, Saitama 351-0198, Japan

³International Institute for Sustainability with Knotted Chiral Meta Matter (WPI-SKCM²), Hiroshima University, 1-3-1 Kagamiyama, Higashi-Hiroshima, Hiroshima 739-8526, Japan

⁴University of California, Berkeley, CA 94720, USA

⁵Department of Materials Science and Engineering,
Texas A&M University, College Station, TX 77843, USA

(Dated: December 8, 2025)

Entangled structures such as textiles, polymer networks, and architected metamaterials are often doubly periodic. Due to this property and their finite transverse thickness, the symmetries of these materials are described by the crystallographic layer groups. While orbifold notation provides a compact topological description and classification of the planar wallpaper groups, no analogous framework has been available for the spatial layer groups. In this article we develop an orbifold theory in three dimensions and introduce a complete set of Conway-type symbols for all layer groups. To illustrate its applicability, we analyze several knitted fabric motifs and show how their layer-group symmetries are naturally expressed in this new orbifold notation. This work establishes a foundation for the topological classification of doubly periodic structures beyond the planar setting and supports structure–function analysis in layered materials.

I. INTRODUCTION

Today, researchers are rapidly expanding the range and application of entangled metamaterials, from engineering efforts towards programmed active textiles [1] to weaving at the molecular scale [2]. Additive manufacturing has enabled the design of new textile materials [3] and other three dimensional architected materials [4]. In order to build a generic framework for understanding and designing entangled metamaterials, there is a need for new mathematical tools to *concisely* describe the symmetries and structures within these increasingly complex materials.

A wide range of these contemporary metamaterials have their topology modeled by doubly periodic entangled structures and exhibit symmetries described not by the two-dimensional wallpaper groups, but by the three-dimensional layer groups [5, 6]. Such structures are periodic in two directions while possessing a finite thickness in the third. Their mechanical and geometric properties are strongly influenced by the symmetry constraints imposed by these subperiodic crystallographic groups [7].

The mathematical study of symmetry in fabrics was significantly advanced by Roth (1993), who analyzed isonemal two-way twofold woven structures [8], and was more recently extended in [9] to include all layer-group symmetries arising in two-way twofold and three-way threefold weaves. Recent developments extended symmetry-based approaches to the study of 2-periodic

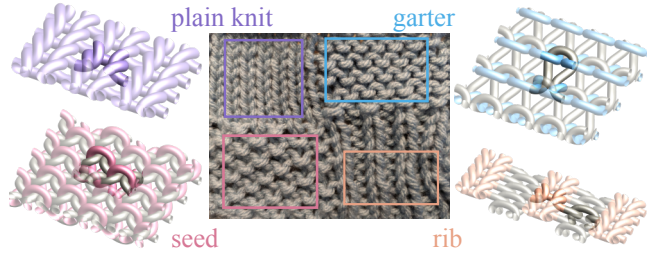


FIG. 1: Fabric swatch with each quadrant a different basic knitted stitch along with a schematic of the stitch structure- upper left stockinette (as known as plain knit or jersey knit), upper right garter stitch, lower left seed stitch and lower right rib stitch.

polycatenane, knit, braid, weave, entangled graph, and crystal patterns [10–14], but these studies did not incorporate orbifold methods. Existing orbifold techniques have been applied in the case of 3-periodic entangled structures, where orbifolds of the hyperbolic plane are muted to be compatible with symmetry of triply periodic minimal surfaces [15–18]. However, there exist no orbifold theory or orbifold theory for the classification of layer groups or for describing 2-periodic entanglement.

In this paper we introduce a new orbifold framework for the symmetry classification of three-dimensional layer groups. While orbifold notation is well-established for the 17 wallpaper groups of the Euclidean plane \mathbb{R}^2 , no analogous symbolic description existed for the 80 layer groups, whose actions occur on the thickened plane $\mathbb{R}^2 \times I$. In Sec. II we review the orbifold theory of wallpaper groups. In Sec. III we extend the orbifold con-

* sonia.mahmoudi@tohoku.ac.jp

struction and the associated cost formalism to the three-dimensional setting of the layer groups, identifying the irreducible symmetries. Mathematically, we obtain a compact and coordinate-independent notation that encodes the topology of the quotient space directly. This provides a new classification tool for any layered materials modeled by doubly periodic structure, such as woven and knitted textiles, polymer networks, metamaterials, where the topology of the underlying pattern is an essential descriptor alongside the crystallographic symmetry.

After establishing this general layer orbifold framework, in Sec. IV we illustrate its effectiveness through a detailed analysis of relevant knitted structures. Knitted fabrics provide a rich family of three-dimensional doubly periodic entangled structures exhibiting nontrivial layer-group symmetries. Previous works on the intersection of knitted fabrics and mathematics have focused on knot theory [19–21]. Here we focus on spatial symmetries of the three-dimensional shape of knitted fabric that emerge from coupling the underlying knot structure with the conditions necessary for mechanical equilibrium. The four basic knitted stitches are shown in Fig. 1, both their schematic structure and their presentation in fabric. To describe knitted fabrics beyond the simplest stitch, stockinette, we must consider the thin third dimension of the fabric. Here we consider these stitches through the lens of the extended orbifold framework developed in Sec. III and find that this is an apt means to describe these materials’ structures and symmetries.

II. ORBIFOLD OF 2D WALLPAPER GROUPS

Doubly periodic tilings of the Euclidean plane \mathbb{R}^2 are classified by symmetry groups preserving the underlying pattern, namely their wallpaper symmetry groups. The isometries of \mathbb{R}^2 consist of translations, rotations, reflections, and glide reflections. In particular, a *wallpaper group* is a discrete group of isometries of \mathbb{R}^2 containing two linearly independent translations. By the crystallographic restriction theorem, a wallpaper group may contain only rotations of order 2, 3, 4, or 6. It is known that there exist 17 wallpaper groups. All classical results recalled in this section are detailed in [22].

Each wallpaper group admits a fundamental domain, and the action of the group identifies edges and vertices of this domain to produce a compact quotient space. A *fundamental domain* is a minimal region of the pattern from which the entire tiling can be generated by applying the symmetries of the group. More intuitively, one may think of it as the smallest piece of the pattern, or smallest ‘tile’, needed to cover the whole plane by applying the symmetries of the group without overlaps or gaps. Unlike a crystallographic unit cell, which is determined purely by translations, a fundamental domain also reflects rotational, reflectional, or glide symmetries.

The identifications on the boundary of a fundamental domain naturally produce a compact quotient space, in

which rotation centers, mirror lines, and glide reflections appear as singular or non-orientable features. Following Thurston, an *orbifold* is a generalization of a surface that records precisely this quotient structure encoding symmetry. For a wallpaper group G , the quotient $O = \mathbb{R}^2/G$ is a compact two-dimensional orbifold. Classifying wallpaper groups is therefore equivalent to classifying the possible orbifold structures that arise from such quotients.

The topology of the underlying surface X_O of an orbifold O is determined by its orientable or non-orientable genus together with the number of boundary components. By the classification of compact surfaces, its Euler characteristic is given by:

$$\chi(X_O) = \begin{cases} 2 - 2g - b, & \text{if } X_O \text{ is orientable,} \\ 2 - k - b, & \text{if } X_O \text{ is non-orientable,} \end{cases} \quad (1)$$

where g is the number of orientable handles, k the number of non-orientable (twisted) handles (crosscaps), and b the number of boundary components. In the quotient of a wallpaper group, translations generate handles of X_O , mirrors produce the boundary components, and glide reflections introduce crosscaps.

In addition to the topology of the underlying surface X_O , an orbifold O of a wallpaper group may carry singular points arising from rotational symmetries: cone points, corresponding to isolated rotational centers of order n , and corner reflectors, corresponding to rotational centers of order n lying on mirror boundaries. These singularities modify the Euler characteristic of X_O : a cone point of order n removes $(1 - \frac{1}{n})$ from $\chi(X_O)$, while a corner reflector of order n removes $\frac{1}{2}(1 - \frac{1}{n})$ from $\chi(X_O)$.

Combining the topology of the underlying surface with the contributions of the singularities gives the Euler characteristic of the orbifold:

$$\chi(O) = \chi(X_O) - \sum_{i=1}^r \left(1 - \frac{1}{a_i}\right) - \frac{1}{2} \sum_{j=1}^s \left(1 - \frac{1}{b_j}\right), \quad (2)$$

where a_1, \dots, a_r are the orders of the cone points and b_1, \dots, b_s the orders of the corner reflectors.

Since \mathbb{R}^2 has Euler characteristic 0, every wallpaper orbifold satisfies $\chi(O) = 0$. In view of equations (1) and (2), the underlying surfaces X_O arising as quotients of wallpaper groups are precisely the sphere S^2 , the disk D^2 , the projective plane \mathbb{RP}^2 , the torus T^2 , the Klein bottle K , the annulus $S^1 \times I$, and the Möbius band Mb .

Conway introduced a symbolic notation that encodes the topology and singular data of a two-dimensional orbifold. For wallpaper groups, the relevant symbols are: $*$ for the presence of mirror boundary, n for a cone point or a corner reflector of order n (where numbers appearing to the right of $*$ denote corner reflectors), \times for a crosscap, and o for the case with only translational symmetry.

In Conway’s combinatorial theory, each character in the orbifold symbol is assigned a numerical *cost* c :

$$\text{cost}(o) = 2, \quad \text{cost}(*) = 1, \quad \text{cost}(\times) = 1,$$

$$\text{cost}(\text{cone } n) = 1 - \frac{1}{n}, \quad \text{cost}(\text{corner } n) = \frac{1}{2} \left(1 - \frac{1}{n}\right),$$

with cone and corner contributions matching the geometric terms appearing in equations (1) and (2). These symbolic costs are chosen so that the Euclidean condition $\chi(O) = 0$ is simply encoded. The *Magic Theorem* states that the symbols satisfying this constraint, that is, the symbols of total cost 2, are precisely those that arise from wallpaper symmetry groups, and that each wallpaper group has a unique orbifold symbol.

III. ORBIFOLDS OF 3D LAYER GROUPS

A. Preliminaries on Layer Groups

The layer groups are the three-dimensional analogues of the wallpaper groups: they describe the symmetries of patterns that are periodic in two directions (doubly periodic) but may vary transversely across a finite thickness. They act by isometries in the thickened plane $\mathbb{R}^2 \times I$, where I denotes the unit interval. As in the planar case, a layer group admits a planar lattice of translations, but the additional transverse direction introduces symmetry operations not present in two dimensions. They form one of the crystallographic subperiodic families, consisting of three-dimensional crystallographic groups with only two independent translational directions. There are exactly 80 layer groups [5].

To encode these symmetry operations in a compact and topologically meaningful way, we introduce Conway-inspired symbols adapted to the layer-group setting. Each symbol encodes the topological effect of the corresponding isometry on the quotient $(\mathbb{R}^2 \times I)/G$, generalizing the role played by orbifold symbols in two dimensions. For vertical mirror planes, glide planes, rotations about axes perpendicular to the layer, and the case of pure translations, we retain the planar symbols, namely $*$, \times , $n = 2, 3, 4, 6$, and o , respectively. Figure 2 illustrates the newly introduced symbols.

These additional symbols arise from symmetry operations that have no analogue in the planar wallpaper setting but become unavoidable in three dimensions. An in-plane 2-fold axis may act either as a pure rotation ($\tilde{2}$) or as a screw rotation involving a half-translation along the axis ($\vec{2}$). Inversion centers ($\bar{1}$) and roto-inversions ($\bar{n} = \bar{3}, \bar{4}, \bar{6}$) similarly appear only when in-plane mirror are combined with rotations, generating singularities similar to the planar cone points. Finally, mirrors and glides parallel to the layer (\odot and \otimes , respectively) must be marked separately from those perpendicular to it, because they contribute differently in the quotient orbifold. Together, these symbols provide a complete description of all possible singular features of a layer-group action, extending the planar Conway notation while preserving its geometric and combinatorial clarity.

Table I lists the symbols used in this paper together with the corresponding isometries of $\mathbb{R}^2 \times I$. This nota-

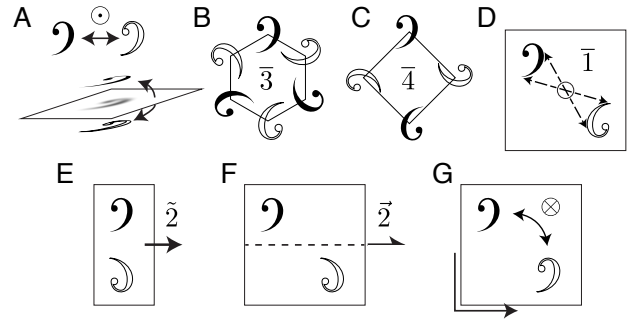


FIG. 2: (A) In-plane mirror: \odot ; (B) 3-fold rotoinversion: $\bar{3}$; (C) 4-fold rotoinversion: $\bar{4}$; (D) Inversion center: $\bar{1}$; (E) In-plane 2-fold rotation: $\bar{2}$; (F) In-plane 2-fold screw rotation: $\vec{2}$; (G) In-plane glide: \otimes .

tion forms the foundation for the orbifold description of layer groups developed in the subsequent sections.

Symbol	Corresponding isometry of $\mathbb{R}^2 \times I$
o	No symmetry other than translations.
\times	Vertical glide plane: 3D extension of a planar glide-reflection axis.
$*$	Vertical mirror plane: 3D extension of a planar mirror axis.
$n = 2, 3, 4, 6$	n -fold rotation about a cone axis or a dihedral edge perpendicular to the layer plane: 3D extension of planar cone points and corner reflectors.
$\tilde{2}$	In-plane 2-fold rotation: rotation about an axis parallel to the layer.
$\vec{2}$	In-plane 2-fold screw rotation: in-plane 2-fold rotation combined with translation along the axis.
$\bar{1}$	Inversion center.
$\bar{n} = \bar{3}, \bar{4}, \bar{6}$	Roto-inversion of order n : n -fold rotation combined with inversion.
\odot	In-plane mirror: mirror plane parallel to the layer.
\otimes	In-plane glide reflection: glide plane parallel to the layer.

TABLE I: Symbols and corresponding symmetry operations used for the orbifold notation of layer groups.

B. Orbifolds of Layer Groups

Let L be a crystallographic layer group acting on the thickened plane $\mathbb{R}^2 \times I$, where I denotes the unit interval. The quotient $O = (\mathbb{R}^2 \times I)/L$ is a compact three-

dimensional orbifold. As in the planar setting, we denote by X_O the underlying compact 3-manifold obtained by forgetting the singular structure.

Thickening a wallpaper orbifold does not change the Euler characteristic of its underlying space. Since I is contractible, we have $\chi(I) = 1$, and therefore

$$\chi(X_O) = \chi(X_{O_W} \times I) = \chi(X_{O_W}) \chi(I) = \chi(X_{O_W}),$$

where $O_W = \mathbb{R}^2/W$ is the orbifold of a wallpaper group W with underlying surface X_{O_W} . Thus the underlying manifold of a layer orbifold has the same Euler characteristic as the underlying surface of its wallpaper planar projection, given by equation (1) of the previous section.

The singular features of a layer-group action consist of rotation axes (thickened cone points), dihedral edges (thickened corner reflectors), and isolated inversion or roto-inversion points. Accordingly, the Euler characteristic of a layer-group orbifold is:

$$\begin{aligned} \chi(O) = \chi(X_O) & - \sum_{i=1}^r \left(1 - \frac{1}{a_i}\right) \\ & - \frac{1}{2} \sum_{j=1}^s \left(1 - \frac{1}{b_j}\right) \\ & - \sum_{\ell=1}^t \left(1 - \frac{1}{c_\ell}\right), \end{aligned} \quad (3)$$

where a_1, \dots, a_r are the orders of the rotation axes, b_1, \dots, b_s the orders of the dihedral edges, and c_1, \dots, c_t the orders of isolated inversion or roto-inversion points.

Since layer groups act by Euclidean isometries on the thickened plane, the resulting orbifold is flat and therefore satisfies $\chi(O) = 0$. Combined with equations (1) and (3), this forces the underlying 3-manifold X_O to be one of the thickened surfaces arising from the planar wallpaper projection, namely: the thickened sphere: $S^2 \times I$, the thickened disk: $D^2 \times I$, the thickened projective plane: $\mathbb{RP}^2 \times I$, the thickened torus: $T^2 \times I$, the thickened Klein bottle: $K \times I$, the thickened annulus: $(S^1 \times I) \times I$, and the thickened Möbius band: $\text{Mb} \times I$.

C. The Magic Cost

To compute the Euler characteristic of a layer orbifold, we assign to each symbol presented in Table I a numerical cost measuring the topological deficit contributed by its singular feature. Since a layer orbifold is obtained by thickening the orbifold of its two-dimensional projection, the Euler characteristic of the underlying manifold is unchanged, as explained above. Consequently, the total cost to be balanced by the singularities is analogous to the planar setting. The following Table II lists the cost associated with each orbifold symbol for layer groups together with the justification inherited from its planar projection.

Symbol	Cost	Justification
o	2	Same base cost as in 2D (torus case).
\times	1	Corresponds to a 2D glide edge and keeps the Conway cost 1.
$*$	1	Projects onto a 2D mirror edge: the boundary-component contribution remains 1.
$n = 2, 3, 4, 6$	$1 - \frac{1}{n}$	Projects onto a 2D cone point or corner reflector of order n , contributing $(1 - \frac{1}{n})$ and $\frac{1}{2}(1 - \frac{1}{n})$, respectively.
$\tilde{2}$	1	The planar projection acts as a reflection and thus holds the cost 1 as for $*$.
$\vec{2}$	1	The planar projection acts as a glide reflection and thus holds the cost 1 as for \times .
$\bar{1}$	$\frac{1}{2}$	The planar projection acts as a 2-fold rotation and thus holds the cost $\frac{1}{2}$ as for 2.
$\bar{n} = \bar{3}, \bar{4}, \bar{6}$	$1 - \frac{1}{k}$	The planar projection acts as a n -fold rotation n composed with an inversion so $\bar{3}$ is of order 6, $\bar{4}$ is of order 4 and $\bar{6}$ is of order 3.
\odot	0	Does not add to the cost beyond that of the 2D projection.
\otimes	0	Does not add to the cost beyond that of the 2D projection.

TABLE II: Costs for layer-group orbifold symbols using the parent-budget convention.

Note that in-plane mirrors and in-plane glides (\odot and \otimes) introduce no new singularities in the orbifold sense: an in-plane mirror simply duplicates the layer as two equivalent boundary components, and an in-plane glide adds only a parallel translation. Neither affects the Euler characteristic of the underlying manifold. For this reason they contribute zero to the orbifold deficit:

$$c(\odot) = c(\otimes) = 0.$$

With these conventions, the sum of all symbol costs ensures that the total orbifold cost of the layer group agrees with that of its wallpaper planar projection, and hence equals 2.

D. The Orbifold Symbols of Layer Groups

We now present the classification of the 80 layer groups using our new orbifold notation. This provides a symbolic system that complements the traditional Hermann–Mauguin (HM) notation. The HM notation, introduced to standardize crystallographic symmetry descriptions, encodes the geometric symmetry operations acting on a chosen conventional unit cell. While this framework is important for crystallography, it does not record the topology of the quotient space obtained from the group action. Our orbifold notation fills this gap by encoding the topology of a minimal fundamental domain of a layer group uniquely. This framework is well suited for modeling and classifying 3D doubly periodic structures, where the topology of the underlying network is a key descriptor alongside the crystallographic symmetry.

The symmetry operations and properties of the layer groups are detailed in the *International Tables for Crystallography, Volume E* (Kopský & Litvin, 2010), hereafter referred to as ITE [5]. Each layer group is identified by a unique number and by its HM symbol, which form the first two columns of our classification Tables III and IV. The initial letter of the HM symbol specifies the centering type of the conventional unit cell (primitive p or centered c), while the following characters describe the symmetry elements acting along the principal directions.

Every layer group admits a canonical planar projection obtained by forgetting the transverse structure and retaining only the in-plane symmetries. This projection preserves all symmetry features that act within the layer, while collapsing purely three-dimensional features such as in-plane mirrors, in-plane glides, in-plane rotations, or screw displacements parallel to the layer into their two-dimensional counterparts. This projection is used solely to relate the layer group to its 2D planar orbifold, whose Euler characteristic and symbolic cost were analyzed in the preceding subsections. The third column of Tables III and IV record the 2D wallpaper group corresponding to the projection of the layer group, given both in HM notation and in the associated Conway symbol of the resulting two-dimensional orbifold.

The fourth and fifth column of Tables III and IV list our new orbifold symbol for each layer group and the corresponding underlying manifold. This symbol is unique, determined entirely by the singular features of the action of the group on the thickened plane. Note that the orbifold of a layer group may sometimes differ from the asymmetric unit as given in the ITE, in particular when the latter is only defined on the upper half plane, generating sharp discontinuity in the pattern, since an orbifold would contain the full thickness. A concrete example is presented in Section IV (see garter stitch in Figure 5).

The assignment of symbol costs established in Table II shows that each orbifold of layer groups satisfies the same cost condition as its planar projection: since thickening a 2D wallpaper orbifold preserves the Euler characteristic of its underlying space, the total deficit contributed

by all singularities of a layer orbifold must be the same, and no further singular terms can appear in three dimensions. This extends Conway’s Magic Theorem to the layer-group setting and ensures both the existence and the uniqueness of the orbifold symbol: for each layer group, there is exactly one symbol with total cost 2.

N.	HM symbol	2D W.P.	Orb.	Und. Man.
1	$p1$	$p1(o)$	o	$T^2 \times I$
2	$p\bar{1}$	$p2(2222)$	$\bar{1}\bar{1}\bar{1}\bar{1}$	$S^2 \times I$
3	$p112$	$p2(2222)$	2222	$S^2 \times I$
4	$p11m$	$p1(o)$	$\odot o$	$T^2 \times I$
5	$p11a$	$p1(o)$	$\otimes o$	$T^2 \times I$
6	$p112/m$	$p2(2222)$	$\odot 2222$	$S^2 \times I$
7	$p112/a$	$p2(2222)$	$\otimes 2222$	$S^2 \times I$
8	$p211$	$pm(**)$	$\tilde{2}\bar{2}$	$(S^1 \times I) \times I$
9	$p2_111$	$pg(\times \times)$	$\bar{2}\bar{2}$	$K \times I$
10	$c211$	$cm(\times \times)$	$\tilde{2}\bar{2}$	$Mb \times I$
11	$pm11$	$pm(**)$	$**$	$(S^1 \times I) \times I$
12	$pb11$	$pg(\times \times)$	$\times \times$	$K \times I$
13	$cm11$	$cm(\times \times)$	$*\times$	$Mb \times I$
14	$p2/m11$	$pmm(*2222)$	$*\bar{1}\bar{1}\bar{1}\bar{1}$	$D^2 \times I$
15	$p2_1/m11$	$pmg(22*)$	$\bar{1}\bar{1}*$	$D^2 \times I$
16	$p2/b11$	$pmg(22*)$	$\bar{1}\bar{1}\tilde{2}$	$D^2 \times I$
17	$p2_1/b11$	$pgg(22\times)$	$\bar{1}\bar{1}\times$	$\mathbb{RP}^2 \times I$
18	$c2/m11$	$cmm(2*22)$	$\bar{1}\ast\bar{1}\bar{1}$	$D^2 \times I$
19	$p222$	$pmm(*2222)$	$\tilde{2}2222$	$D^2 \times I$
20	$p2_122$	$pmg(22*)$	$22\bar{2}$	$D^2 \times I$
21	$p2_12_12$	$pgg(22\times)$	$22\bar{2}$	$\mathbb{RP}^2 \times I$
22	$c222$	$cmm(2*22)$	$2\tilde{2}22$	$D^2 \times I$
23	$pmmm2$	$pmm(*2222)$	$*2222$	$D^2 \times I$
24	$pma2$	$pmg(22*)$	$22*$	$D^2 \times I$
25	$pba2$	$pgg(22\times)$	$22\times$	$\mathbb{RP}^2 \times I$
26	$cmm2$	$cmm(2*22)$	$2*\bar{2}2$	$D^2 \times I$
27	$pm2m$	$pm(**)$	$\odot **$	$(S^1 \times I) \times I$
28	$pm2_1b$	$pm(**)$	$\otimes **$	$(S^1 \times I) \times I$
29	$pb2_1m$	$pg(\times \times)$	$\odot \times \times$	$K \times I$
30	$pb2b$	$pm(**)$	$\otimes \tilde{2}\bar{2}$	$(S^1 \times I) \times I$
31	$pm2a$	$pm(**)$	$*\tilde{2}$	$(S^1 \times I) \times I$
32	$pm2_1n$	$cm(\times \times)$	$\otimes *\bar{2}$	$Mb \times I$
33	pb_21a	$pg(\times \times)$	$\otimes \times \bar{2}$	$K \times I$
34	$pb2n$	$cm(\times \times)$	$\otimes \bar{2}\times$	$Mb \times I$
35	$cm2m$	$cm(\times \times)$	$\odot *\times$	$Mb \times I$
36	$cm2e$	$pm(**)$	$\otimes *\tilde{2}$	$(S^1 \times I) \times I$
37	$pmmm$	$pmm(*2222)$	$\odot *2222$	$D^2 \times I$
38	$pmaa$	$pmm(*2222)$	$\odot *\bar{1}\bar{1}\bar{1}\bar{1}$	$D^2 \times I$
39	$pban$	$cmm(2*22)$	$\otimes \bar{1}\tilde{2}22$	$D^2 \times I$
40	$pmam$	$pmg(22*)$	$\odot 22*$	$D^2 \times I$

TABLE III: Orbifold classification table for layer groups (1-40) listing: the ITE number (N.), its HM symbol, the wallpaper projection (2D W.P.), the orbifold symbol (Orb.), and the underlying manifold (Und. Man.).

N.	HM symbol	2D W.P.	Orb.	Und. Man.
41	<i>pmma</i>	$pmm(*2222)$	$\otimes * 2\bar{2}\bar{1}\bar{1}$	$D^2 \times I$
42	<i>pman</i>	$cmm(2*22)$	$\otimes 2*\bar{1}\bar{1}$	$D^2 \times I$
43	<i>pbaa</i>	$pmg(22*)$	$\otimes \bar{1}\bar{1}\bar{2}$	$D^2 \times I$
44	<i>pbam</i>	$pgg(22\times)$	$\odot 22\times$	$\mathbb{RP}^2 \times I$
45	<i>pbma</i>	$pmg(22*)$	$\otimes 22*$	$D^2 \times I$
46	<i>pmmn</i>	$cmm(2*22)$	$\otimes \bar{1}*22$	$D^2 \times I$
47	<i>cmmm</i>	$cmm(2*22)$	$\odot 2*22$	$D^2 \times I$
48	<i>cmme</i>	$cmm(2*22)$	$\otimes 2*22$	$D^2 \times I$
49	<i>p4</i>	$p4(442)$	$\bar{4}42$	$S^2 \times I$
50	<i>p4</i>	$p4(442)$	$\bar{4}\bar{4}2$	$S^2 \times I$
51	<i>p4/m</i>	$p4(442)$	$\odot 442$	$S^2 \times I$
52	<i>p4/n</i>	$p4(442)$	$\otimes 442$	$S^2 \times I$
53	<i>p422</i>	$p4m(*442)$	$\bar{2}442$	$D^2 \times I$
54	<i>p4212</i>	$p4g(4*2)$	$4\bar{2}2$	$D^2 \times I$
55	<i>p4mm</i>	$p4m(*442)$	$*442$	$D^2 \times I$
56	<i>p4bm</i>	$p4g(4*2)$	$4*2$	$D^2 \times I$
57	<i>p42m</i>	$p4m(*442)$	$\bar{2}\bar{4}42$	$D^2 \times I$
58	<i>p421m</i>	$p4g(4*2)$	$\bar{4}*2$	$D^2 \times I$
59	<i>p4m2</i>	$p4m(*442)$	$*4\bar{4}2$	$D^2 \times I$
60	<i>p4b2</i>	$p4g(4*2)$	$\bar{4}\bar{2}2$	$D^2 \times I$
61	<i>p4/mmm</i>	$p4m(*442)$	$\odot * 442$	$D^2 \times I$
62	<i>p4/nbm</i>	$p4m(*442)$	$\otimes \bar{2}442$	$D^2 \times I$
63	<i>p4/mbm</i>	$p4g(4*2)$	$\odot 4*2$	$D^2 \times I$
64	<i>p4/nmm</i>	$p4m(*442)$	$\otimes * 442$	$D^2 \times I$
65	<i>p3</i>	$p3(333)$	333	$S^2 \times I$
66	<i>p3</i>	$p6(632)$	$\bar{3}32$	$S^2 \times I$
67	<i>p312</i>	$p3m1(*333)$	$\bar{2}333$	$D^2 \times I$
68	<i>p321</i>	$p31m(3*3)$	$\bar{3}\bar{2}3$	$D^2 \times I$
69	<i>p3m1</i>	$p3m1(*333)$	$*333$	$D^2 \times I$
70	<i>p31m</i>	$p31m(3*3)$	$33*3$	$D^2 \times I$
71	<i>p31m</i>	$p6m(*632)$	$\bar{2}\bar{3}32$	$D^2 \times I$
72	<i>p3m1</i>	$p6m(*632)$	$*\bar{3}32$	$D^2 \times I$
73	<i>p6</i>	$p6(632)$	632	$S^2 \times I$
74	<i>p6</i>	$p3(333)$	$\bar{6}\bar{6}\bar{6}$	$S^2 \times I$
75	<i>p6/m</i>	$p6(632)$	$\odot 632$	$S^2 \times I$
76	<i>p622</i>	$p6m(*632)$	$\bar{2}632$	$D^2 \times I$
77	<i>p6mm</i>	$p6m(*632)$	$*632$	$D^2 \times I$
78	<i>p6m2</i>	$p3m1(*333)$	$\odot * \bar{6}\bar{6}\bar{6}$	$D^2 \times I$
79	<i>p62m</i>	$p31m(3*3)$	$\odot \bar{6}6*\bar{6}$	$D^2 \times I$
80	<i>p6/mmm</i>	$p6m(*632)$	$\odot * 632$	$D^2 \times I$

TABLE IV: Orbifold classification table for layer groups (41-80) listing: the ITE number (N.), its HM symbol, the wallpaper projection (2D W.P.), the orbifold symbol (Orb.), and the underlying manifold (Und. Man.).

IV. SYMMETRIES OF KNITTED FABRICS

We now consider the symmetries in a selection of common textile structures: the four basic knitted stitches. Just as wallpaper symmetries are naturally found in vi-

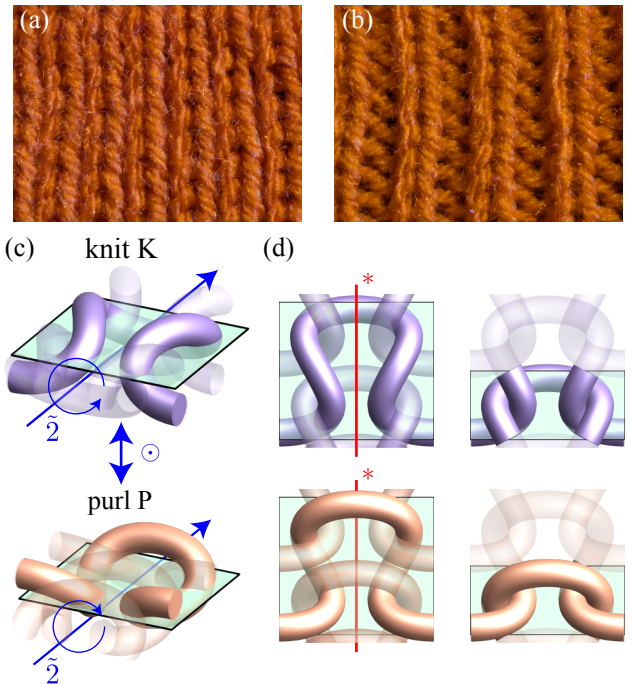


FIG. 3: (a) Rib fabric with no applied forces resembles stockinette fabrics. (b) When rib fabric is stretched in the horizontal direction, its three dimensional structure and layer symmetries are revealed. (c) Knit and purl stitches are related by an in-plane mirror *or* a 2-fold rotation about the axis parallel to the wale direction. (d) Top-down projections of knit and purl stitches; in the case of translational periodicity, each loop can be reduced, given a set of periodic boundaries in the shaded region (right).

sual art that lies on a surface—mosaics, tapestries, and printed patterns, to name a few [23]—knitted and woven textiles are artistic depictions of layer symmetries. However, the full richness of these symmetries are hidden within the thin transverse thickness of the material, with hints of the underlying structure on display as a fabric texture, giving the impression of wallpaper symmetries.

The layer symmetries can instead be *experienced*, to some degree, through the mechanics of these materials. Perhaps the most dramatic presentation of layer symmetries is through rib-knit fabric. The stripe-based texture of rib fabric appears similar to plain-knit (stockinette or jersey) at a first glance. If the material is stretched course-wise then the front stripes separate, showing a striped reversed pattern that alternates with the front-facing pattern. These two strikingly different states of the same fabric are shown in Fig. 3a, b. Notably, this striped patterning gives rise to an extreme mechanical response in rib fabric, resulting in a soft, highly-extensible response when stretched along the course but a much stiffer response along the wale [24].

While there is a variety of stitches that can be employed by a knitter, the most basic are the ‘knit’ (K)

and the ‘purl’ (P). The knit stitch, shown in fig. 3c, joins neighboring courses (rows) of yarn through a slip knot that loops behind the fabric, whereas the purl has a loop that lies in front of the fabric. A separate *reduced* representation of a stitch consists, shown in the right panels of fig. 3d, defines a stitch as the pair of claps formed by segments of two separate courses of yarn; as we explore below, this reduced representation is equivalent to the former when stitch symmetry permits the use of periodic stitch boundaries to identify free ends of each yarn segment. Each stitch, if excised from the surrounding fabric, only contains a single point symmetry: a mirror plane that cuts transverse to the plane of the fabric and lies along the wale direction ($*$ in the orbifold notation). Any ‘rectangular’ swatch of purely K/P-patterned fabric whose stitches can be organized by a direct product of m wales and n courses maintains these mirror planes along the wales. Furthermore, the K and P stitches are related by either a mirror operation through the plane of the fabric (i.e., an action of \odot) or through a π -rotation of the fabric about the wale axis (i.e., an action of $\tilde{2}$), as shown in Fig. 3c,d. Note that the two operations that interconvert between K and P are identical only if the stitches maintain their wale-wise mirrors. In cases where this symmetry is broken, as happens when the yarn has a preferred twist [25, 26], care must be taken in how to relate K and P. In the case of circular knitting, where the swatch forms a cylinder, allowing for unambiguous definition of a front and reverse side of the fabric, K and P are related by a mirror operation through the fabric. Meanwhile, in the case of linear knitting, the yarn direction is reversed each time a course is completed—often involving switching fabric orientation when hand knitting—so K and P are related by a π rotation about the wale axis. Other ways of removing mirror symmetries involves twisted versions of these stitches or altering the swatch lattice so that it is no longer a direct product of wale and course directions. This latter change can be accomplished, for example, by knitting two stitches in one row together to form a single stitch in the next row or by using short rows, resulting in defect structures analogous to edge dislocations in crystals.

In many ways, the simplest knitted fabric is the plain knit, also known as the stockinette or Jersey, shown in the upper left quadrant of Fig. 1 and Fig. 4a. When viewed from the font of the fabric, in the knitting convention, a plain knit is a rectangular lattice of K stitches (fig. 4a). Foregoing discussion of fabric boundaries—cast on, bind off, edges, or joins—we will limit our discussion to infinite patterns. In this case, the wale-wise mirror (symbol: $*$) is joined by a pair of new two-fold axes (symbol: 2) that pierces through the plane of the fabric. These separate two-fold axes are centered at the center of a yarn-yarn crossing or ‘clasp’ as well as the midpoints of the wale-wise connecting segments of yarn. The mirror symmetry, combined with each of these two-fold axes, creates a pair of glide planes through the fabric. These symmetry operations are shown in Fig. 4b. As a result, the layer

group is identified as pma2, in agreement with [27]. The fundamental domain of the fabric is identified as half of a yarn-yarn clasp, shown in Fig. 4c. Focusing on the mirror along with the pair of two-fold axes as fundamental generators of the symmetry group, we find that the orbifold signature is $22*$, which is consistent with the layer group identification. As shown in Fig. 4d-g, the full translational unit cell can be constructed from the symmetry elements acting on the fundamental domain. Note that both the layer group and orbifold identification mark the plane knit as a structure that has purely 2D symmetries—that is, pma2 is also a wallpaper group.

The garter stitch is obtained by alternating courses of pure K and P, as shown in the upper right quadrant of Fig. 1 and Fig. 5a. We analyze the case where the fabric is slightly stretched in the wale direction, revealing the full texture of the fabric in a manner analogous to the unfolding of the rib fabric shown in Fig. 3a,b. In this rectangular fabric setting, we can regard that P stitch as being obtained from K by translation along the wale by a single stitch, half of a translational unit, followed by an in-plane mirror (\odot). As a result, the fabric has a glide symmetry parallel to the plane, which we denote by \otimes . Similar to the plain knit, the garter has two-fold axes in the centers of the yarn-yarn clasp regions. However, as shown in Fig. 5b, the new parallel glide symmetry converts the two-fold axis placed midway along the wale-wise connecting yarn segments into inversion centers, denoted $\bar{1}$. As a result there is only a single independent glide plane passing perpendicular through the fabric along the course direction. The combination of wale-wise mirror and inversion center generates parallel screw axes (denoted $\tilde{2}$) along the wale direction, with axes collinear with the mirror planes, along with separate parallel screws along the course direction, aligned with the perpendicular glide planes. We identify the orbifold (Fig. 5c), which is bounded by pairs of mirrors and two-fold axes. As shown in Fig. 5e, this orbifold can generate the remainder of the translational unit cell. However, we emphasize that the orbifold is not the ‘minimal unit’ of the structure: a smaller asymmetric unit can be created under a further quotient of the orbifold by the inversion operation $\bar{1}$, as shown in Fig. 5d. Note that the inclusion of this operation is not compatible with the definition of an orbifold as it would only consider the upper-half of the fundamental domain. We identify garter as orbifold $\otimes 22*$, and hence layer group pbma (in agreement with [27]). However, the reduced asymmetric unit gives additional insight into the construction of garter and illustrates that fact that the orbifold representation not always ‘fully minimal’.

Next, consider our initial example of the stretched rib pattern, which is a relative of garter where wales alternate between pure K and P, shown in the lower right quadrant of Fig. 1 and Fig. 6a. While similar to garter, rib is characterized only by perpendicular mirrors, an in-plane glide, and in-plane two-fold rotations (see Fig. 6b). Notably, unlike the plain knit and garter, the underlying

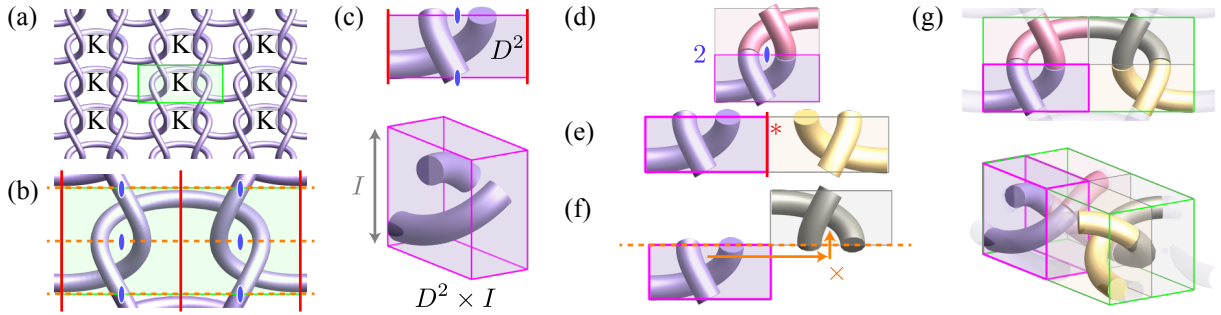


FIG. 4: (a) Representation of the plain knit as a doubly-periodic tiling of space using just knit (K) stitches. The unit cell is boxed in green. (b) Close-up of the translational unit cell, highlighting two-fold axes (blue ellipses), perpendicular mirrors (red solid lines), and perpendicular glide planes (orange dashed lines). (c) Fundamental domain, along with identification of the underlying manifold as $D^2 \times I$. Illustrations of actions on the fundamental domain: (d) a two-fold rotation, (e) perpendicular mirror, and (f) perpendicular glide. (g) Translational unit cell (outlined in green) tiled by fundamental domains (outlined in pink).

manifold for rib, is based on a thickened annulus $S^1 \times I$ rather than the extrusion of a disk D^2 . This is because the rib pattern lacks the perpendicular two-fold axes of plain knit and garter. The fundamental domain, shown in Fig. 6c, therefore extends the full width of the translational unit cell along the wale direction, adopting a single set of periodic boundaries. Finally, much like the garter pattern, the resulting rib structure adopts distinct top and bottom layer components, as shown in Fig. 6d. We identify rib as the orbifold $\otimes * \tilde{2}$, corresponding to layer group pm2a. It is interesting to note that the this presentation of the rib knit as a stacked structure with only half of each layer filled relies on the coarse-stretched configuration shown here; the relaxed rib structure in Fig. 3a fills in these voids.

Our final example is seed, shown in the lower left quadrant of Fig. 1, which consists of an alternating ‘checkboard’ pattern of K and P (see Fig. 7a). This has the largest unit cell of the typical knit patterns, consisting of a pair of Ks and pair of Ps. As depicted in Fig. 7b, the checkerboard structure gives rise to orthogonal pairs of in-plane glide symmetries. The remaining symmetries are all wale-oriented, much like rib, and consists of in-plane screw axes aligned with the perpendicular mirrors, along with in-plane two-fold axes aligned with perpendicular glide planes. The fundamental domain for seed is perhaps the least intuitive, consisting of a single layer of curve segments that belong to separate knit and purl stitches. This domain, shown in Fig. 7c, is much like rib in that it is based on a thickened annulus as it spans a single translational direction. However, since the screw symmetry involves a half-translation along the wale direction, as shown in Fig. 7d, the image of this domain not only lies in the complementary layer, but is similarly translated by half a unit cell along the wale direction. As a result the image of the highlighted fundamental domain under symmetry actions gives rise to a distinctly staggered translational unit cell, shown in Fig. 7e. In accordance with the convention of constructing convex polyhe-

dral translational units, the portions of fundamental domains that hang outside of the conventional rectangular (i.e. extruded rectangular cuboid) unit cell are wrapped through the unit cell boundary, giving rise to the structure in Fig. 7f. Since the in-plane screw, in-plane glide, and mirror operations generate the translational unit, we identify the orbifold as $\otimes * \tilde{2}$, which is layer group cm2e (in agreement with [14]).

Finally, we discuss implications of these bulk symmetries on the boundaries of the fabric. In rib and seed stitches, mirror symmetry is broken along half of the mirror planes for which it existed in garter and stockinette stitches, and this instead becomes a two-fold rotation axis pointing along the wale direction. The direction of fabric loops along these two-fold rotation axes points to the direction that the fabric was cast-on. Thus, by examining only a single unit cell of rib or seed fabric one can determine its direction of origin, a distinction impossible in garter or stockinette fabric.

V. CONCLUSION

An orbifold framework for the 80 crystallographic layer groups is presented in this article, extending the classical Conway notation from the planar wallpaper groups to the three-dimensional setting of the thickened plane. By introducing new symbols for the singular features unique to layer-group actions and establishing a cost formalism that generalizes Conway’s Magic Theorem, we obtained a complete, coordinate-independent, and topologically meaningful classification. This provides a compact description of the quotient spaces associated with layer-group symmetries and complements the traditional Hermann–Mauguin notation.

To illustrate the applicability of this framework, we analyzed the symmetry of common knitted patterns, showing how their layer-group symmetries are naturally cap-

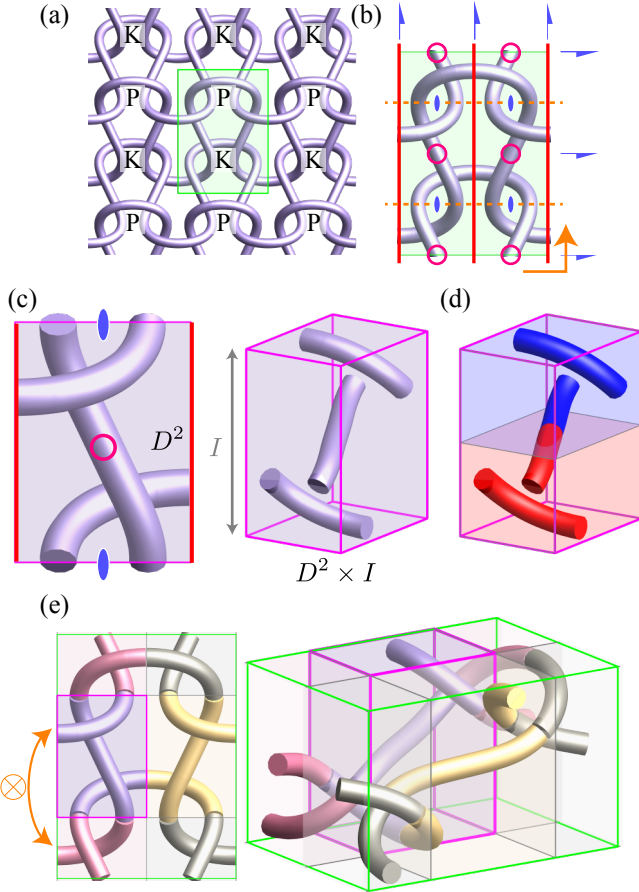


FIG. 5: (a) Representation of the garter stitch as a doubly-periodic tiling of space using alternating courses of knit (K) and purl (P) stitches. (b) Close-up of the translational unit cell, highlighting two-fold axes (blue ellipses), perpendicular mirrors (red solid lines), perpendicular glide planes (orange dashed lines), inversion centers (pink circles), the parallel glide symmetry (orange arrow), and in-plane screw axes (blue half-arrows). (c) Orbifold, along with identification of the underlying manifold as $D^2 \times I$. (d) Asymmetric unit obtained by quotient of the orbifold by the inversion operation. (e) Translational unit cell tiled by fundamental domains, along with a depiction of an in-plane glide.

tured by the new orbifold symbols. These examples demonstrate how the notation can support the study of doubly periodic structures in materials science, where geometry, connectivity, and symmetry jointly influence material behaviour. The framework developed here opens the way for future investigations, including the systematic classification of woven and knitted textiles as well as chainmail [28–30], the analysis of periodic entanglement in engineered materials, and broader applications to doubly periodic structures arising in mathematics and

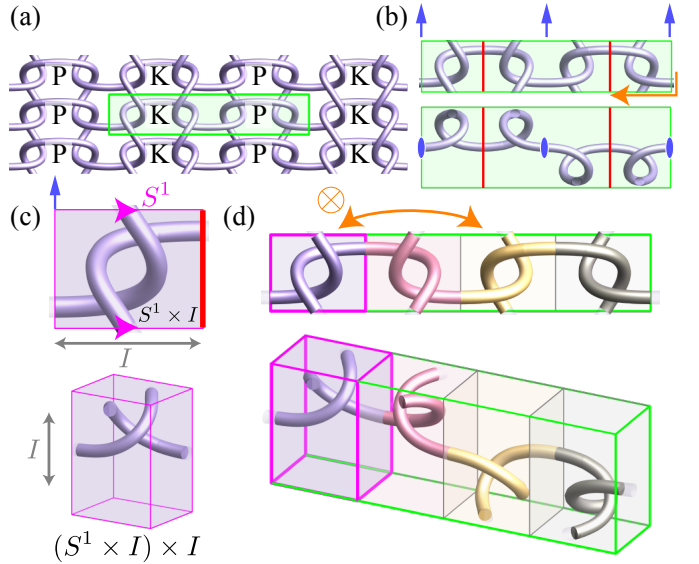


FIG. 6: (a) Representation of the rib stitch as a doubly-periodic tiling of space using alternating wales of knit (K) and purl (P) stitches. (b) Close-up of the translational unit cell, the above schematic in-plane and below schematic with horizontal axis along the course and vertical axis along the thickness of the fabric, highlighting perpendicular mirrors (red solid lines), the parallel glide symmetry (orange arrow), and in-plane two-fold axes (blue arrows/ellipses). (c) Fundamental domain, along with identification of the underlying manifold as $(S^1 \times I) \times I$. (d) Translational unit cell tiled by fundamental domains, along with a depiction of an in-plane glide.

physics.

Recent work [24] has shown that the internal, sub-unit cell symmetries of knitted fabrics play key roles in determining the macroscopic response of fabrics. In particular, in a reduced elastica model of 2D projections of the full 3D yarn shape, it was found that curve segments exhibiting ‘even symmetry’ are stiffer than segments exhibiting ‘odd symmetry’ by an order of magnitude. Since the K/P arcs that pass through the perpendicular mirror planes have even symmetry, all stitches contain at least some of these stiffer elements. Furthermore, similar ‘even’ arcs can be found at the boundaries between neighboring K stitches and neighboring P stitches. However, the curve segments between neighboring K/P stitches were found to have odd symmetry profiles. This simple model provides rationale for the extreme anisotropic elastic response of the different knit patterns as well as reasonable predictions for the comparative magnitude of fabric stiffnesses. The binary decomposition of curves into even and odd shapes used in this analysis is only applicable in a 2D approximation of the curve shapes. Our analysis of knitted structures using full layer symmetries is the first step towards a potential generalization of this prior work, where distinct responses for curve segments

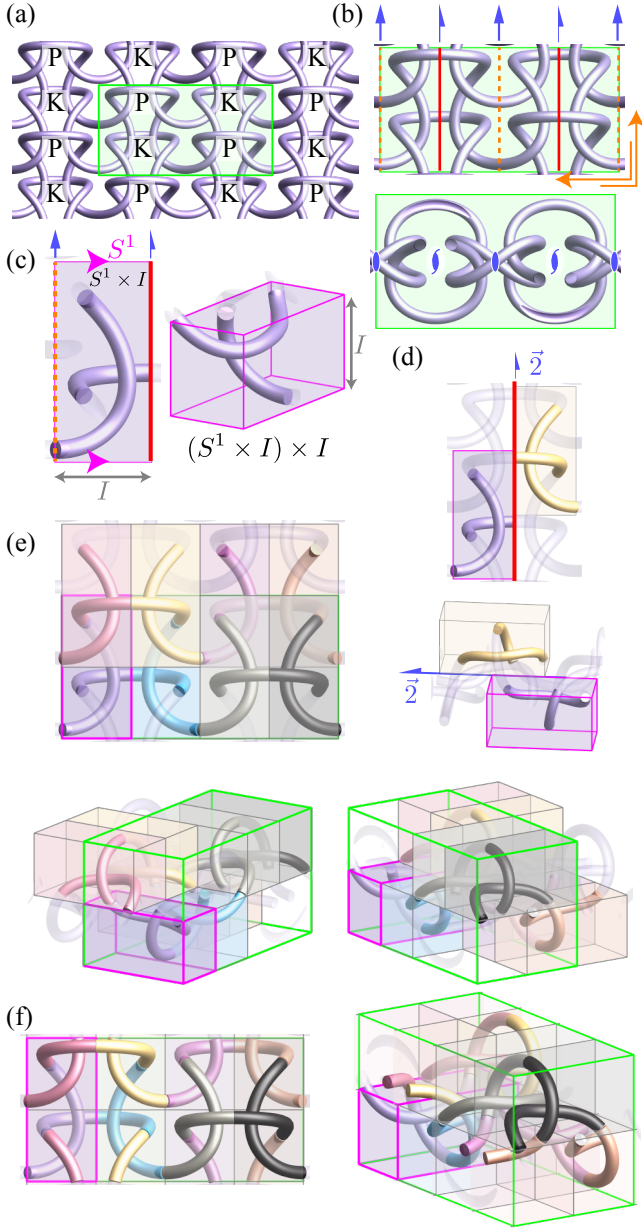


FIG. 7: (a) Representation of the seed stitch using a checkerboard pattern of knit (K) and purl (P) stitches. (b) Top-down and side views of the translational unit cell, highlighting perpendicular mirrors (red solid lines), perpendicular glide planes (orange arrows), the parallel glide symmetries (orange dashed lines), in-plane two-fold axes (blue arrows/ellipses), and in-plane screw axes (blue half-arrows/swirls). (c) Fundamental domain, along with identification of the underlying manifold as the thickened annulus $(S^1 \times I) \times I$. (d) Illustration of the in-plane screw acting on a fundamental domain. (e) Wrapping of the fundamental domains into the conventional unit cell.

Construction of a translational unit cell tiled by fundamental domains; note that half of the domains involve a shift through the unit cell boundaries due to the action of the in-plane screw. (f) Wrapping of the fundamental domains into the conventional unit cell.

with local mirror, inversion, and rotational point group symmetries could be used to construct a more complete coarse-grained mechanical model of knitted fabrics. This would complement additional recent work on elasticity and other tensorial properties of anisotropic doubly periodic materials which were determined using representation theorems and shown to be highly dependent on the wallpaper group of the material [31].

Finally, molecular weaving structures have been classified into layer groups with an abstraction into nodes joined by links [7]. This abstraction, however, hides symmetries that may be present within the links and nodes themselves, and may be important for some material properties. The extended orbifold framework we introduce here will be valuable in applying the aforementioned and a multitude of findings pertaining to the symmetry-based classification of material properties to layered materials.

ACKNOWLEDGEMENTS

This article is dedicated to Stephen T. Hyde, whose influential contributions to the study of orbifold symmetry in triply periodic entangled structures and their applications in chemistry were an important source of inspiration for this work.

The authors also thank Elisabetta Matsumoto for valuable discussions regarding the symmetry classification of knitted fabrics.

The first author is supported by JSPS KAKENHI Grant-in-Aid for Early-Career Scientists (Grant Number 25K17246) and the Daiichi-Sankyo “Habataku” Support Program for the Next Generation of Researchers 2025. She also acknowledges financial support from the Tohoku Forum for Creativity of Tohoku University, the Japan Tourism Agency (MICE), and the Sendai Tourism, Convention and International Association (SenTIA) for supporting the program *The Theory of Periodic Tangles and Their Interdisciplinary Applications*, during which a significant part of this research was developed.

The second author acknowledges support from the National Science Foundation (Grant No. CMMI-2344589), the College of Chemistry at UC Berkeley, and the support of Sanjay Govindjee and Kranthi Mandadapu.

COMPETING INTERESTS

We declare we have no competing interests.

[1] V. Sánchez, C. J. Walsh, and R. J. Wood, Textile technology for soft robotic and autonomous garments, *Advanced Functional Materials* **31**, 2008278 (2021).

[2] Y. Liu, Y. Ma, Y. Zhao, X. Sun, F. Gándara, H. Furukawa, Z. Liu, H. Zhu, C. Zhu, K. Suenaga, P. Oleynikov, A. Alshammari, X. Zhang, O. Terasaki, and O. M. Yaghi, Weaving of organic threads into a crystalline covalent organic framework, *Science* **351**, 365 (2016).

[3] E. M. Keefe, J. A. Thomas, G. A. Buller, and C. E. Banks, Textile additive manufacturing: An overview, *Cogent Engineering* **9**, 2048439 (2022).

[4] W. Zhou, S. Nadarajah, L. Li, A. G. Izard, H. Yan, A. K. Prachet, P. Patel, X. Xia, and C. Daraio, 3d polycatenated architected materials, *Science* **387**, 269 (2025).

[5] V. Kopský and D. B. Litvin, The 80 layer groups, in *International Tables for Crystallography Volume E: Subperiodic groups*, edited by V. Kopský and D. B. Litvin (Springer Netherlands, Dordrecht, 2002) pp. 219–389.

[6] S. Mahmoudi and M. Fukuda, A symmetry invariant for classifying doubly periodic tangles (in preparation).

[7] Y. Liu, M. O’Keeffe, M. M. J. Treacy, and O. M. Yaghi, The geometry of periodic knots, polycatenanes and weaving from a chemical perspective: a library for reticular chemistry, *Chemical Society Reviews* **47**, 4642 (2018).

[8] R. L. Roth, The symmetry groups of periodic isonemal fabrics, *Geometriae Dedicata* **48**, 191 (1993).

[9] M. L. A. De Las Peñas, M. Tomenes, and K. Liza, Symmetry groups of two-way twofold and three-way threefold fabrics, *Acta Crystallographica Section A* **80**, 33 (2024).

[10] M. O’Keeffe and M. M. J. Treacy, Crystallographic descriptions of regular 2-periodic weavings of threads, loops and nets, *Acta Crystallographica Section A* **76**, 110 (2020).

[11] M. E. Evans and S. T. Hyde, Symmetric tangling of honeycomb networks, *Symmetry* **14**, 10.3390/sym14091805 (2022).

[12] M. O’Keeffe and M. M. J. Treacy, Isogonal 2-periodic polycatenanes: chain mail, *Acta Crystallographica Section A* **80**, 86 (2024).

[13] J. Fu, M. Kuusma, A. H. Larsen, K. Shinohara, A. Togo, and K. S. Thygesen, Symmetry classification of 2d materials: layer groups versus space groups, *2D Materials* **11**, 035009 (2024).

[14] S. Takano, Y. Kochi, K. Yoshida, E. A. Matsumoto, Y. Kotorii, T. Asahi, and K. Inoue, Chiral analogues of knit stitches designed using chiral topology (2025), arXiv:2509.23604.

[15] M. E. Evans, V. Robins, and S. T. Hyde, Periodic entanglement i: networks from hyperbolic reticulations, *Acta Crystallographica Section A* **69**, 241 (2013).

[16] M. E. Evans, V. Robins, and S. T. Hyde, Periodic entanglement ii: weavings from hyperbolic line patterns, *Acta Crystallographica Section A* **69**, 262 (2013).

[17] M. E. Evans and S. T. Hyde, Periodic entanglement iii: tangled degree-3 finite and layer net intergrowths from rare forests, *Acta Crystallographica Section A* **71**, 599 (2015).

[18] B. Thompson and S. T. Hyde, A theoretical schema for building weavings of nets via colored tilings of two-dimensional spaces and some simple polyhedral, planar and three-periodic examples, *Israel Journal of Chemistry* **58**, 1144 (2018).

[19] D. S. Shimamoto, K. Shimamoto, S. Mahmoudi, and S. Poincloux, *Topological defect propagation to classify knitted fabrics* (2025), 2506.22369.

[20] S. Markande and E. Mastumoto, Knotty knits are tangles on tori (2020), arXiv:2002.01497.

[21] S. Grishanov, V. Meshkov, and A. Omelchenko, A topological study of textile structures part II: topological invariants in application to textile structures, *Textile Research Journal* **79**, 822 (2009).

[22] J. H. Conway, H. Burgiel, and C. Goodman-Strauss, *The Symmetries of Things* (CRC Press, 2008).

[23] B. Grünbaum, What symmetry groups are present in the alhambra, *Notices of the AMS* **53**, 670 (2006).

[24] K. Singal, M. Dimitriev, S. Gonzalez, S. Quinn, A. P. Cachine, and E. Mastumoto, Programming Mechanics in Knitted Materials, Stitch by Stitch, *Nature Communications* **15** (2024).

[25] A. Pavko-Čuden, Skewness and spirality of knitted structures., *Tekstilec* **58** (2015).

[26] Y. Inui, H. Wakamatsu, E. Morinaga, and E. Arai, Prediction of skewness for plain-knitted fabric based on the modeling of knitted structure, in *2017 IEEE/SICE International Symposium on System Integration (SII)* (2017) pp. 793–798.

[27] M. O’Keeffe and M. M. J. Treacy, Isogonal piecewise-linear embeddings of 1-periodic knots and links, and related 2-periodic chain-link and knitting patterns, *Acta Crystallographica Section A: Foundations and Advances* **78**, 234 (2022).

[28] F. A. Farris, Wallpaper patterns from nonplanar chain mail links, in *Bridges 2020 Conference Proceedings* (Tessellations Publishing, 2020) pp. 183–190.

[29] F. A. Farris, Wallpaper patterns from looping strands: The layer groups, *Proceedings of Bridges* **71** (2021).

[30] A. R. Klotz, C. J. Anderson, and M. S. Dimitriev, Chirality effects in molecular chainmail, *Soft Matter* **20**, 7044 (2024).

[31] E. J. Dresselhaus, S. Govindjee, and K. K. Mandadapu, Anomalous tensorial properties of anisotropic 2D materials (2025), arXiv:2508.20055.